Journal of Photochemistry & Photobiology, A: Chemistry 440 (2023) 114666

Contents lists available at ScienceDirect

Journal of Photochemistry & Photobiology, A: Chemistry

journal homepage: www.elsevier.com/locate/jphotochem

Solvation structure and dynamics of a small ion in an organic electrolyte

Shivshankar Kore [a,b], Rudhi Ranjan Sahoo [c,d], Binit Santra [e], Archishman Sarkar [f], Tubai Chowdhury [a,b], Samadhan H. Deshmukh [a,b], Sulagna Hazarika [a], Srijan Chatterjee [a,b,*], Sayan Bagchi [a,b,*]

[a] Physical and Materials Chemistry Division, National Chemical Laboratory (CSIR-NCL), Dr. Homi Bhabha Road, Pune 411008, India
[b] Academy of Scientific and Innovative Research (AcSIR), Ghaziabad 201002, India
[c] School of Chemical Sciences, National Institute of Science Education and Research (NISER), Bhubaneswar 752050, India
[d] Homi Bhabha National Institute, Training School Complex, Anushakti Nagar, Mumbai 400094, India
[e] Department of Chemistry, Indian Institute of Technology Kanpur, Kanpur 208016, India
[f] School of Applied and Interdisciplinary Sciences, Indian Association for the Cultivation of Science, 2A Raja SC Mullick Road, Kolkata, West Bengal 700032, India

A B S T R A C T

Organic carbonates are commonly used as electrolytes in commercial lithium-ion batteries. A detailed interpretation of the solvation structure and dynamics of the electrolyte around ions is necessary to understand the charge/discharge process in batteries. This work combines infrared absorption spectroscopy with quantum chemical calculations and molecular dynamics simulations to decipher the solvation structure of propylene carbonate, a cyclic carbonate, around the dissolved thiocyanate ion. Two dimensional infrared spectroscopy and polarization-selective pump probe spectroscopies have been utilized to extract the timescales of solvent fluctuation and the solute reorientational dynamics. The similarity in the slow timescales for the solute and the solvent dynamics signifies that similar processes control both dynamics.

1. Introduction

Small organic carbonates are finding extensive utility as solvents in synthesis due to their favourable physical characteristics, such as large dipole moment, high polarizability, low ecotoxicity, and good biodegradability.[1] Primarily, these organic carbonates are used as liquid media for electrolytes in lithium-ion batteries (LIBs).[2–4] Among the primary functional components of LIBs, electrolytes play a crucial role in facilitating the movement of lithium ions during electric charge and discharge.[5–8] The properties of the electrolytes such as viscosity and dielectric constant play an important role in the overall transfer of charge.[9,10]

Propylene carbonate (PC), a cyclic organic carbonate, is commonly used in electrolyte solutions of LIBs. The large dipole moment (4.9 D) and high dielectric constant (~64) of PC make it well-suited for non-aqueous electrochemical applications.[11–13] To this end, elucidating the structure and dynamics of PC is important. A recent study investigated the liquid structure of PC using neutron scattering and classical force field based molecular modelling.[14] Additional classical models incorporated scaled atomic charges to mimic polarization effects.[15] Another recent study used ab initio molecular dynamics (AIMD) simulations to investigate the importance of hydrogen bonding in the structure of PC.[16] They inferred that the local structure is dominated by the hydrogen bond motifs. This hydrogen bond motifs gives rise to head to tail bonding, which is in agreement with many of the previous reports.[14,17–19]

However, the main challenge of understanding the organic carbonate arises from the fast timescales of the electrolyte dynamics,[20–22] which is inaccessible by the experimental techniques routinely used to investigate the molecular structure of solutions. For example, it has been reported that the formation and dissociation dynamics of different ionic species are in the picosecond timescale.[23,24] Time-resolved vibrational spectroscopy, with ultrafast time resolution, allows us to investigate the solvation structure and dynamics of small ions in these organic electrolytes.[22,24] Organic carbonates consist of an intrinsic vibrational probe (carbonyl, C = O), which has been recently utilized in time-resolved infrared (IR) spectroscopy to study the solvation shell structure and ion speciation in the electrolytes.[9,20,25] However, vibrational coupling, overlapping C = O peaks arising from free /bound Li^+ ions, and Fermi resonance can make it difficult to interpret the solvation structure and dynamics of these carbonate electrolytes.[21,22,26,27] It has been shown that multiple mechanisms prevent any straightforward analysis of the C = O IR spectra for cyclic carbonates.[28]

In this work, we have used the nitrile stretch of a small pseudohalide

* Corresponding authors.
E-mail addresses: srijan.sc@gmail.com (S. Chatterjee), s.bagchi@ncl.res.in (S. Bagchi).

https://doi.org/10.1016/j.jphotochem.2023.114666
Received 31 August 2022; Received in revised form 28 February 2023; Accepted 5 March 2023
Available online 9 March 2023

anion (thiocyanate, SCN^-) as the vibrational reporter in an organic carbonate, PC. Here, the pseudohalide anion is not used as a replacement of the lithium cation, but as a probe of PC fluctuation dynamics to circumvent the complexities observed previously in the C = O IR spectra. Although the absence of a dissolved lithium salt in the electrolyte apparently bears no relevance toward LIB, the transport process of Li^+ in the battery depends on (1) the Li^+ - solvent interaction and (2) the solvent fluctuation. Use of a small vibrational reporter that absorbs in a solvent-background free frequency region provides direct access to estimating the solvent fluctuation. Pseudohalides, which absorb at a transparent frequency window of the electrolytes, has been successfully utilized to probe the dynamics in another class of battery electrolytes (concentrated aqueous electrolytes) to decipher the ultrafast dynamics using two dimensional IR (2D IR) spectroscopy.[29] Once the fluctuation timescales of the organic carbonates are known, we can turn to the C = O stretch of the Li-salt solutions of organic carbonates in a future work to decipher the solvation structure arising from Li^+ - solvent interaction.

We have combined Fourier transform IR (FTIR) spectroscopy, 2D IR spectroscopy, and polarization selective pump probe (PSPP) spectroscopy to characterize the solvation shell structure of PC around the thiocyanate ion. Our results show experimental signatures of weak hydrogen bond between the thiocyanate ion and the PC molecules, which is well supported by the previous literature. Our experimental results indicate that the ion senses two distinct timescales of solvent dynamics. Interestingly, the orientational relaxation timescale of the ion quantitatively agrees with the bulk solvent fluctuation timescale. The experimental results are combined with density functional theory (DFT calculations) and molecular dynamics (MD) simulations to make our conclusions robust.

2. Materials and methods

2.1. Chemicals and reagents

Ammonium thiocyanate (NH_4SCN), dimethylformamide (DMF), propylene carbonate (PC), dimethyl sulfoxide (DMSO), and deuterium oxide (D_2O) were purchased from Sigma Aldrich and were directly used without further purification.

2.2. FTIR spectroscopy

FTIR spectra were obtained using a Bruker Vertex 70 FTIR spectrometer. The FTIR sample cell was a demountable cell consisting of two calcium fluoride (CaF_2) windows (3 mm thickness) separated by 100 μm mylar spacer. A solution of 50 mM of NH_4SCN was prepared by dissolving it in the respective solvents. ~ 90 μL solution of the prepared solution was loaded between the CaF_2 windows, separated by the spacer, to acquire the FTIR spectra. The spectrum of the neat solvent was subtracted from the respective solutions spectrum to obtain the reported spectrum. Peak positions are obtained by fitting the background subtracted spectra with a Voigt lineshape function using the Opus software (default software of Bruker IR spectrometer).

2.3. 2D IR spectroscopy

The 2D IR spectra were acquired by using a pulse shaper-based 2D IR spectrometer.[30] A detailed description of the setup used for this work has been described in our previous publication.[31] In short, mid IR pulses, centred at ~ 2050 cm^{-1}, were generated with ~ 60 fs pulsewidth. A beam splitter splits the mid IR pulse into a strong pump (80%) beam and a weak probe (20%) beam. An acoustic-optic modulator (AOM) based pulse shaper was used to generate two pump pulses with variable delay intervals of (τ). The spatially and temporally overlapped pump and probe pulses were focused at the sample using parabolic mirrors. A motorised delay stage was used to set the pump and probe delay (T_w). Each 2D IR spectrum was acquired by scanning (τ) at fixed T_w. After the sample position, signal was dispersed using a monochromator and detected using a nitrogen-cooled 64-pixel HgCdTe (MCT) IR array detector. The 2D IR experiments were performed with the same solutions used for the FTIR experiments, in the same sample cell. The group velocity dispersion (GVD) was corrected using the pump–probe signal of the germanium (Ge) wafer to remove any chirp in the IR pulses.

In a typical 2D IR experiment, three ultrashort pulses are used to excite the sample. The initial (excitation) frequencies of the vibrational probe are labelled by the first and second pulses. The structural evolution of the solvent occurring during the time-delay between second and third pulse (T_w) causes the initially labelled frequencies to change. The final (detection) frequencies are plotted against the initial frequencies to obtain a 2D IR spectrum at each T_w. 2D IR spectra are correlation plots between the excitation and the detection frequencies.

2.4. PSPP spectroscopy

Polarization-selective pump probe (PSPP) experiments were performed in the parallel $< xxxx >$ and perpendicular $< xxyy >$ polarization conditions, where the polarization of the pump beam was either parallel or perpendicular with respect to that of the probe beam. Pump polarization before the sample was controlled using the combination of a half wave-plate and a polarizer. The signals obtained from $< xxxx >$ and $< xxyy >$ polarization conditions are denoted by $S_{\|}(t)$ and $S_{\perp}(t)$ respectively, such that

$$S\|(t) = P(t)[1 + 0.8C_2(t)]$$

$$S_{\perp}(t) = P(t)[1 - 0.4C_2(t)]$$

where $C_2(t)$ is the second Legendre polynomial orientational correlation function and $P(t)$ is vibrational lifetime.

2.5. Quantum chemical calculations

Geometries optimization was performed using density functional theory (DFT) with the hybrid functional B3LYP and the 6–31 + G(d,p) basis set.[32] All calculations were performed using the Gaussian 09 program.[33]

2.6. Molecular dynamics simulation

All-atom classical MD simulations were performed using the GROMACS version 2020.4 package.[34] The force field for thiocyanate anion, ammonium cation and PC solvent were modelled using widely used OPLS force field from LigParGen server.[35] One ammonium thiocyanate molecule was solvated by 793 PC molecules to maintain the box size of 50x50x50 $Å^3$. The systems were first energy minimised with steepest decent energy algorithm to avoid any steric clashes. It was further equilibrated (NVT) with velocity rescale thermostat with a time constant of 0.1 ps at 300 K. After the NVT equilibration, NPT equilibration was performed using Parrinello − Rahman barostat maintaining a pressure of 1 bar. Finally, unconstrained production runs of 50 ns (velocity rescale thermostat and Parrinello − Rahman barostat) were performed with position and velocities saved every 1 ps. During the simulation, LINCS algorithms were used to restrain all the covalently bonded hydrogen atoms. Periodic boundary conditions with 16 Å cut off for short-range electrostatic were implemented. RDF calculations were performed using the default tool gmx_rdf in GROMACS. SDF analysis were performed using TRAVIS molecular trajectory analysis software.[36]

3. Solvation structure: Results and discussions

3.1. Absorption spectra

The CN stretch absorption spectrum of NH_4SCN in PC is shown in Fig. 1. The spectrum has a peak around 2057 cm^{-1} and a full width at half maximum (FWHM) of ~ 16 cm^{-1}. To compare the peak position in PC with other solvents, the CN stretch spectra are obtained in other aprotic and protic solvents (Fig. S1a and Table S1). For aprotic solvents, previous reports suggested that increasing solvent polarity causes a larger Onsager reaction field and results in a red-shift of the CN stretching frequency.[37–39] More recently, the CN frequency has been correlated to the electric field exerted by the aprotic solvent on the CN bond through vibrational Stark effect (VSE).[31,39,40] In these previous reports, a consistent red-shift in the CN stretch was reported from THF to DMSO, but a blue-shift was observed for the solute participating in hydrogen bonding with the protic solvent.[38,41] In addition, using DMSO/water mixtures, it was shown that the blue-shift increases with the increase in water concentration of the aqueous binary mixture.

Our solvatochromic results are in agreement with the previous reports (Fig. S2). However, the peak position in PC is blue-shifted from that observed in DMF and DMSO (Fig. S1a). The observed blue-shift in PC is intriguing and can be plausibly explained by the presence of some specific solute–solvent interactions like hydrogen-bonding. However, it is surprising for an aprotic solvent like PC to form a conventional hydrogen bond with the thiocyanate ion. One of the plausible origin of hydrogen bonding can be the formation of contact ion pair between the NH_4^+ cation and the SCN^- anion, where the hydrogen atoms of the cation can form hydrogen bond with anion. Clearly distinguishable peaks from ion pairs and aggregates of the NH_4SCN were previously observed in THF.[24] However, it has been recently reported that the ion pair and aggregate peaks are replaced by a free anion peak at 2055 cm^{-1} in polar solvents like DMF and DMSO.[42,43] We have performed concentration-dependent FTIR of NH_4SCN in PC. No spectral signatures of aggregates and ion pairs were observed up to 100 mM of salt concentration (i.e. no new transitions/peaks was observed). We have chosen to work with 50 mM which is 50% of the salt concentration that did not show any CIP or aggregation. Considering these previous reports, the concentration dependent FTIR (Fig. S3), and the FTIR peak position in PC (2057 cm^{-1}), it is imperative that the NH_4^+ cations are not involved either in ion pair formation or hydrogen bonding.

The FWHM of the CN peak in PC is ~ 3 cm^{-1} and ~ 2.3 cm^{-1} broader than that reported in DMF and DMSO, respectively (Table S1). It has been previously reported that an increase in FWHM can arise from either the increase in polarity or the presence of hydrogen-bonded conformers.[44–47] Additionally, unlike the CN spectra in other aprotic solvents, the CN spectrum in PC could not be fitted to one symmetric peak (Fig. S1b). The dashed curve in Fig. 1 is a fit to a Voigt lineshape function on the blue side of the spectrum. Extending the peak to the red side of the spectrum confirms that the CN peak is asymmetric with a small wing on the red side. Similar observations have been previously reported, and the asymmetric lineshape has been attributed to the non-Condon effect (NCE).[48–50] Previous reports suggested that the solute–solvent hydrogen bonds play an essential role in NCE.[49,50] It has been reported that a qualitative explanation involves the nature of solute–solvent interactions of the thiocyanate ion, determined from the contribution of the two possible resonance structures: $[S-C\equiv N]^-$ and $[S=C=N]^-$. [50] For a hydrogen-bonded thiocyanate ion, the electron density shifts toward the nitrogen atom, increasing the contribution from the $[S-C\equiv N]^-$ resonance structure. It has been previously reported that $[S-C\equiv N]^-$ absorbs at the blue side of the spectrum and has a weaker transition dipole than $[S=C=N]^-$. [50] Thus, NCE is observed due to alteration of local solvation structure as the vibrational transition dipole moment undergoes a notable change from the red to the blue side of the spectrum. Interestingly, the observed NCE also suggests that the thiocyanate ion forms some kind of specific interaction with PC which alters the vibrational transition dipole moment.

3.2. Theoretical calculations

We have performed theoretical calculations to obtain a molecular-level understanding of the formation of any specific interaction between the thiocyanate ion and PC. The distance between the thiocyanate nitrogen atom and a hydrogen atom of the methyl side chain is 2.5 Å (Fig

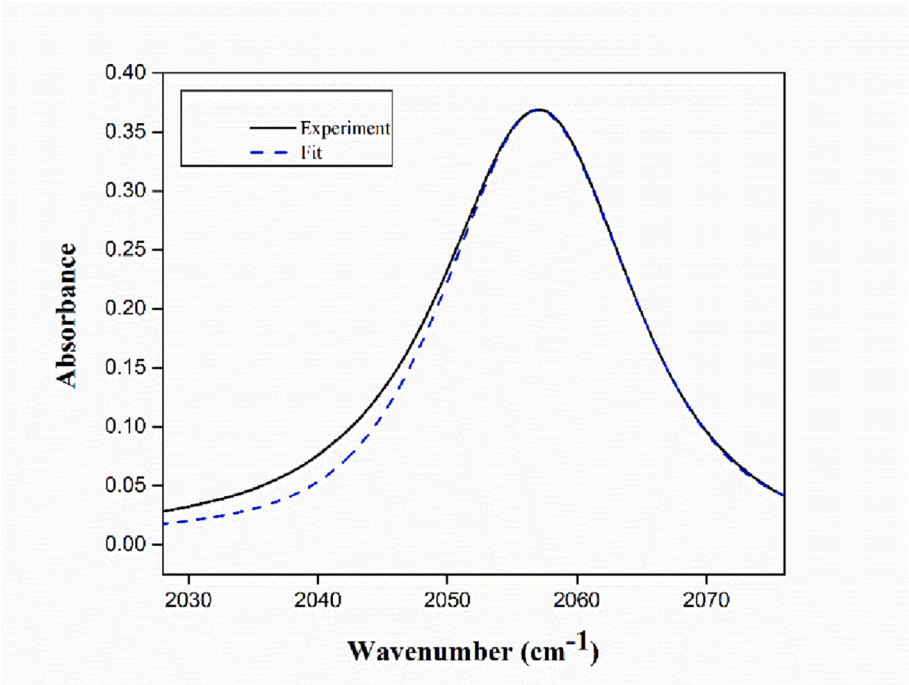

Fig. 1. FTIR spectrum of SCN^- (CN stretch) in propylene carbonate (black) fitted with a Voigt lineshape function (dashed blue). The wing on the red side of the spectrum, arising due to non-Condon effect could not be fitted with the Voigt lineshape function.

S4). The hydrogen atom attached to the ring CH_2 is also found to be within a distance of 2.6 Å. These distances are shorter than the reported distance of ~ 2.9 Å for a non-canonical CH…N hydrogen bond.[51–53] It is important to note that these DFT calculations contain one thiocyanate and one/two PC molecules. However, in solution, several solvent molecules surround the thiocyanate anion. To obtain a more realistic molecular picture in the solution, we have performed MD simulations. The spatial distribution function (SDF) obtained from MD simulations (Fig. 2a) shows that the solvent molecules orient themselves around the ion such that the methyl side chain and the ring –CH_2 in PC are placed nearest to the nitrogen (N) atom of the thiocyanate. For a quantitative interpretation of the MD results, we have obtained two different radial distribution functions g(r): (1) between the N atom of the SCN^- and the methyl side chain and (2) between the N atom and the ring CH_2 (Fig. 2b). Our results show that the average distance between the N atom and the ring CH_2 is 2.8 Å, which is shorter than the non-canonical CH…N hydrogen bond. However, the average distance between the N atom and the methyl side chain is slightly longer (3 Å) than that reported for CH…N hydrogen bond. We have also looked into the radial distribution function between the N atom and the ring C atom (C_3 in Fig. 2c). Our calculations show that the average C…N distance is 3.7 Å. This distance indicates that the CH…N interaction between SCN^- and PC is a weak hydrogen bond.[54] In a recent publication[16] using AIMD, Beck and co-workers have predicted that the primary intermolecular interaction in neat PC is the CH…O hydrogen bonding interaction between the carbonyl oxygen and the ring hydrogens. They have also commented that classical MD underestimates the hydrogen bonding interactions as compared to AIMD. They have stated that these CH…O hydrogen bonds are the primary intermolecular interactions in PC which is responsible for the chain forming structure, i.e., where the individual molecules line up behind one another facing a common direction, as seen from neutron diffraction experiments.[14] In another recent report, Kalugin and co-workers[55] predicted weak CH…O intermolecular hydrogen bonding interactions in PC.

Distance is just one of the criteria for CH…N hydrogen bond formation. We have also looked into the distribution of H-C-N angle. There is a small population (~20%) that satisfies both the distance and the angle criteria (<30°) of hydrogen bonds. Beck and co-workers also reported a broad angular distribution of the CH…O interaction.[16] Therefore, the experimentally observed blue-shift and asymmetry in the FTIR spectrum, when combined with the recent theoretical reports, hint at a plausible weak CH…N hydrogen bond interaction between the thiocyanate anion and the solvent. However, further experimental and theoretical (outside the scope of this work) studies would be required to conclusively determine the hypothesis of specific interaction.

4. Solvation dynamics: Results and discussions

4.1. 2D IR spectroscopy

The instantaneous frequency for the CN stretch of a thiocyanate ion in PC is determined by the solvation environment through intermolecular solute–solvent interactions. The presence of many solute molecules in the ensemble gives rise to a frequency distribution as observed in the Fig. 1. Heterogeneity in the solvent configurations around the thiocyanate ion contributes to various frequency sub-ensembles within the broad FTIR spectrum. As the solvent structures evolve in time, these frequency sub-ensembles exchange on the timescales of the solvent fluctuations, giving rise to spectral diffusion. T_w-dependent 2D IR spectroscopy allows direct extraction of the spectral diffusion timescales.

A typical 2D IR spectrum consists of a peak-pair corresponding to ground-state bleach and stimulated emission (blue peak, v = 0 to v = 1), and excited-state absorption (red peak, v = 1 to v = 2) separated along the detection axis by vibrational anharmonicity. Fig. 3 shows the 2D IR spectra of the thiocyanate ion in PC at different T_w values. At a small T_w, the excitation and the detection frequencies are correlated and the peaks appear to be elongated along the diagonal. As T_w increases, the correlation is gradually lost due to solvent fluctuations, the peaks broaden, and the diagonal-tilt decreases. At a large T_w, when the entire conformational space is sampled, the spectrum resembles a circular peak shape.

The spectral diffusion timescales are extracted from the T_w-dependent 2D IR spectra. Frequency-frequency correlation function (FFCF), which connects the experimental observables to the underlying dynamics, are estimated using the nodal line slope (NLS) method.[56] Although different methods, namely NLS and center line slope (CLS) are used to extract the FFCF from T_w-dependent 2D IR spectra, a recent report has mentioned that although both the methods are equivalent in the absence of noise, NLS is more robust.[57] NLS, shown in Fig. 4, refers to inverse of the slope of the nodal line between the 0–1 and 1–2 peaks. In the absence of a homogeneous contribution at $T_w = 0$, the excitation and detection frequencies are perfectly correlated and the nodal line is parallel to the diagonal, rendering a NLS value of 1. At a large T_w, when the correlation is completely lost, the peaks become vertical, and the NLS value is zero. However, any homogeneous contribution, arising from the vibrational lifetime and the motionally narrowed component produced by very fast structural fluctuations, causes the NLS value at $T_w = 0$ to be less than unity. As pulse overlap can cause spectral distortions, the smallest T_w value reported here is 250 fs. Fig. 4 shows that the NLS value at $T_w = 250$ fs is < 0.5. The NLS decay is fitted to a bi-exponential decay function (Table S2), NLS = 0.24 exp(-T_w/1.4) + 0.28 exp(-T_w/10.7). The sum of the two amplitudes ($a_1 + a_2$ in Table S2) indicate that the NLS value at $T_w = 0$ is 0.52. The time-components show a fast

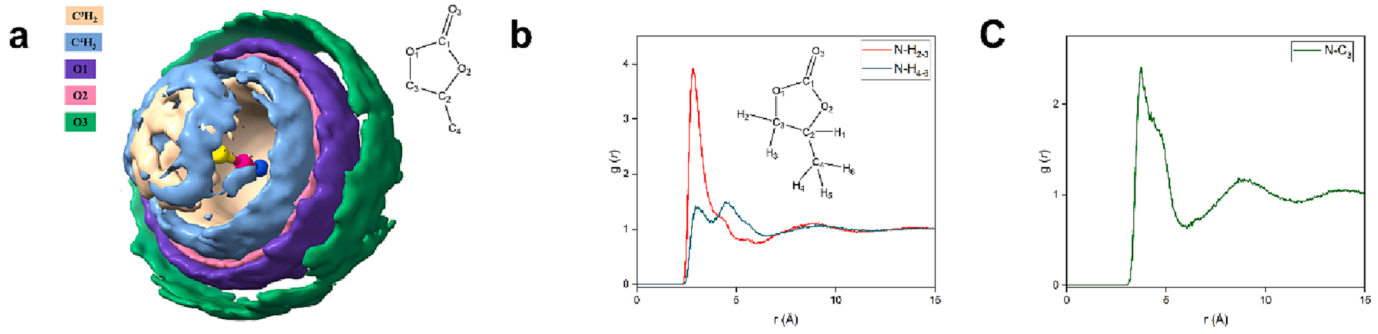

Fig. 2. A)Spatial Distribution Function (SDF) of PC around SCN^-. The colour representation for the respective PC atoms is shown. For SCN^-, Yellow represents the sulphur atom, pink represents the carbon atom, and blue represents the nitrogen atom. The numbering of the atoms is also shown. (b) Radial distribution functions g (r) between (1) the N atom of the SCN^- and the methyl side chain (red) and (2) the N atom and the ring CH_2 (dark cyan). The first peak is observed at 2.8 Å (dark cyan) and 3.0 Å (red), respectively. (c) Radial distribution function g(r) between the hydrogen donor (Carbon) and hydrogen acceptor (Nitrogen).

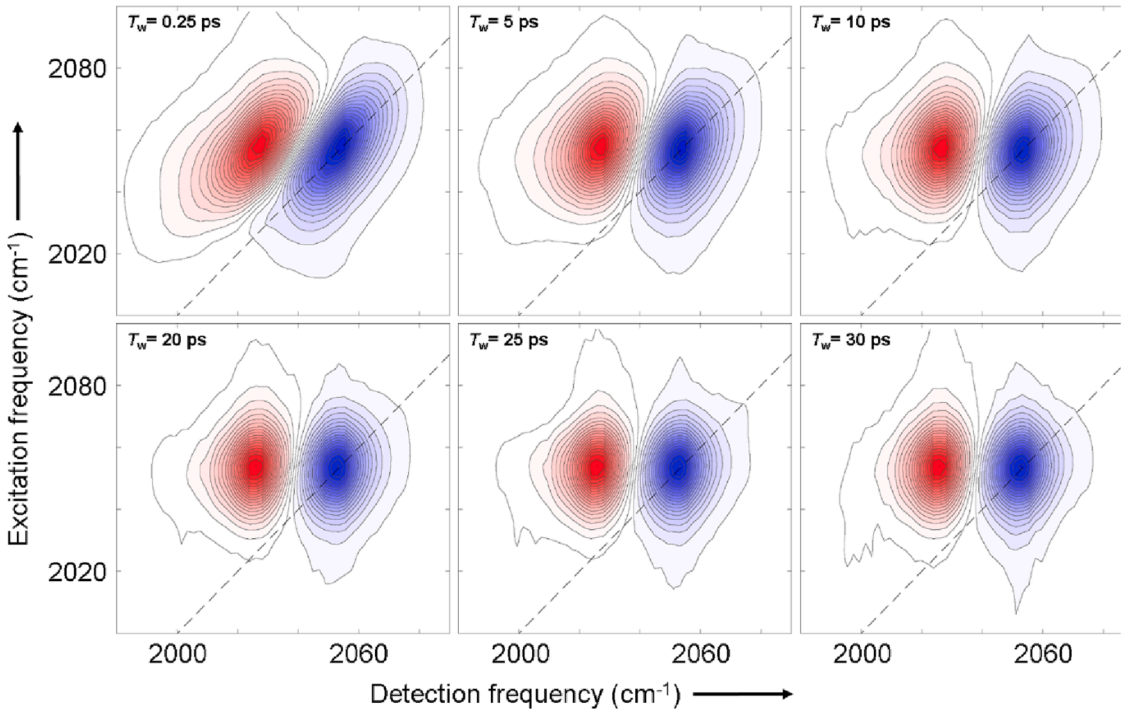

Fig. 3. 2D IR spectra of SCN^- in PC at different waiting times (T_w).

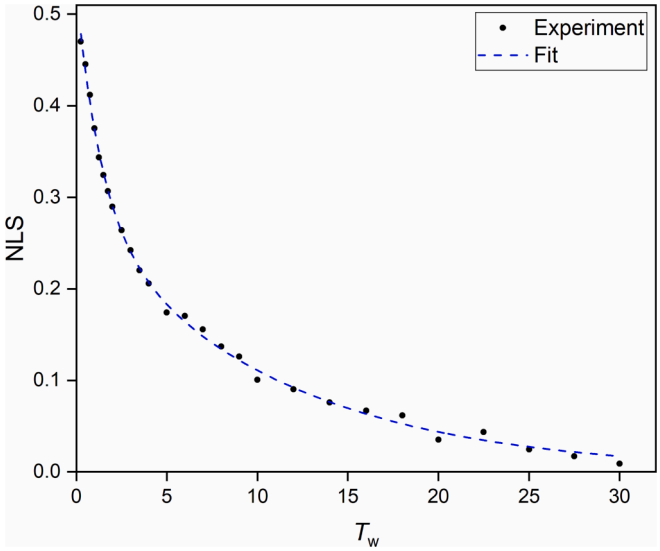

Fig. 4. NLS decay of SCN^- in PC with increasing T_w (black points). The decay is fitted to a bi-exponential decay function (dashed blue) NLS = 0.24 exp (-t/1.4) + 0.28 exp (-t/10.7), R^2 = 0.99.

timescale (τ_f) of ~ 1.5 ps and a slow timescale (τ_s) of ~ 11 ps. The presence of two distinct timescales indicate two different dynamical processes contribute to the fluctuations of PC. A fast solvation dynamics timescale of 2 ps in PC has been previously reported.[58] Solvent fluctuation in this timescale will plausibly alter any preferential solvation environment (first solvation shell) around the solute. We therefore attribute τ_f to the local fluctuations around the solute. Solute reorientation dynamics (discussed later) corroborates with this explanation. On the other hand, the reported FFCF timescale in DMF of SCN^- shows a single fluctuation timescale (5 ps).[43] Therefore, the slow timescale can be assigned to the bulk dynamics of the solvent.[59,60]

4.2. PSPP spectroscopy

PSPP experiments measure the vibrational population relaxation and orientational relaxation of the solute. The orientational relaxation is very sensitive to the transience of the local solvent structures around the solute, as time-dependent changes in the solvation structure can enable a greater extent of orientational relaxation. Combinations of $S_{\|}(t)$ and $S_{\perp}(t)$ provide expressions for $P(t)$ and the anisotropy $r(t)$, as follows:

$$P(t) = \frac{1}{3}[S\|(t) + 2S_{\perp}(t)]$$

$$r(t) = \frac{S\|(t) - S_{\perp}(t)}{S\|(t) + 2S_{\perp}(t)} = 0.4C_2(t)$$

From the PSPP measurement, the vibrational lifetime of the thiocyanate ion in PC is observed to be bi-exponential with timescales of ~ 3 ps (65%) and ~ 40 ps (35%). Interestingly, the lifetime decay show frequency-dependence (Fig. 5). A similar frequency-dependence was previously reported as a direct experimental evidence of NCE.[50] The observed frequency-dependence confirms the origin of the small wing in the red side of the FTIR spectrum. Fig. 5 shows the short time P(t) data at two wavelengths. An initial fast decay is observed on the red side of the absorption spectrum (red points), whereas, the decay curve at the blue side of the spectrum (denoted by blue points) shows a slower decay. An explanation of this phenomenon can be given as follows.

Because the molecules on the red side of the spectrum have larger transition dipoles than those on the blue side, they get over-pumped by the pump pulse, i.e., greater number of molecules get excited in the red side than it would be based solely on the fact that structural configurations are what giving rise to these transition frequencies. Thus, the pump pulses produce a non-equilibrium situation, with an excess of the excited state population on the red side of the FTIR spectrum as compared to the blue side. So, at initial timescales, more molecules flow from red to blue than from blue to red through spectral diffusion in order to re-establish the equilibrium. For a spectral diffusion timescale of 1.5 ps and a vibrational lifetime of 37.4 ps, it has been previously reported that NCE causes a rise in the blue population.[50] However, thiocyanate

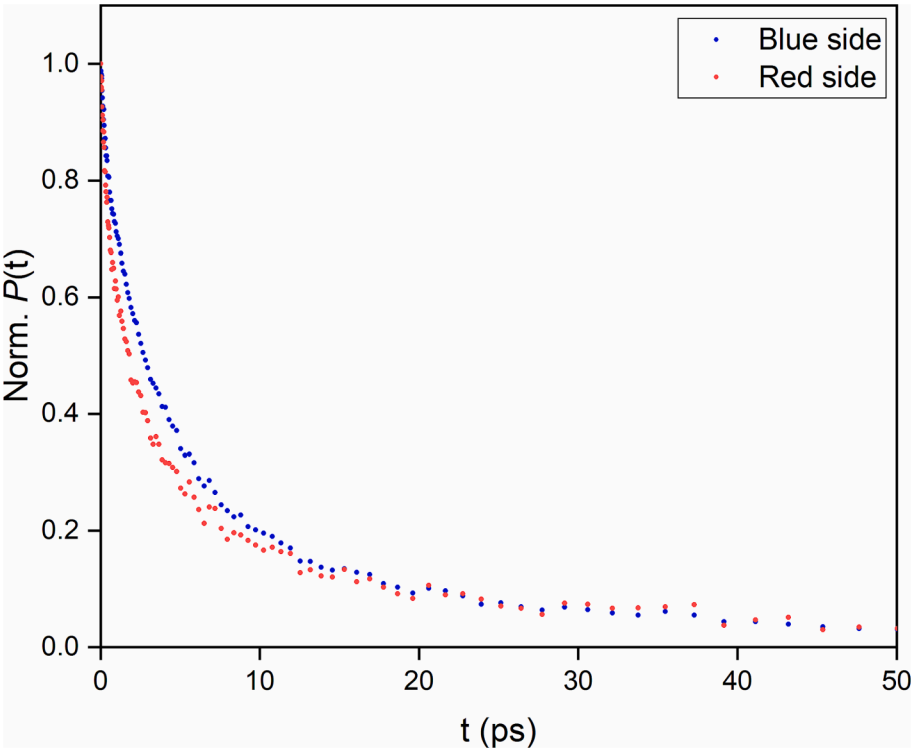

Fig. 5. Normalized frequency-dependent vibrational relaxation at the red (red points) and the blue side (blue points) of the FTIR spectrum.

in PC has comparable timescales of spectral diffusion and vibrational lifetime and therefore the rise on the blue side could not be observed even though the NCE is present.

Fig. 6 shows the anisotropy decay of the thiocyanate anion in PC. The anisotropy has a maximum value of 0.4 and a minimum value of zero. The initial drop from 0.4, observed in our PSPP experiments, arises from an ultrafast inertial decay with a time constant faster than the experimental resolution.[61] The anisotropy decay fits to a bi-exponential function (Table S3), which is dominated by a timescale of 12 ps. The fast timescale of ~ 1 ps (with a small amplitude) indicates some steric restrictions that prevent complete orientational randomization. The fast decay can be explained by the well-established wobbling-in-a-cone model.[49] The timescale of ~ 1 ps indicates that the fluctuation of the first solvation shell (preferential solvation) might be playing a role in the initial wobble. However, the complete randomization of the thiocyanate ion needs the rearrangement of the first few solvation shells of PC. The similar timescales observed for spectral diffusion and solute reorientation elucidates that the solute orientation cannot completely randomize until all solvent structural configurations are sampled.

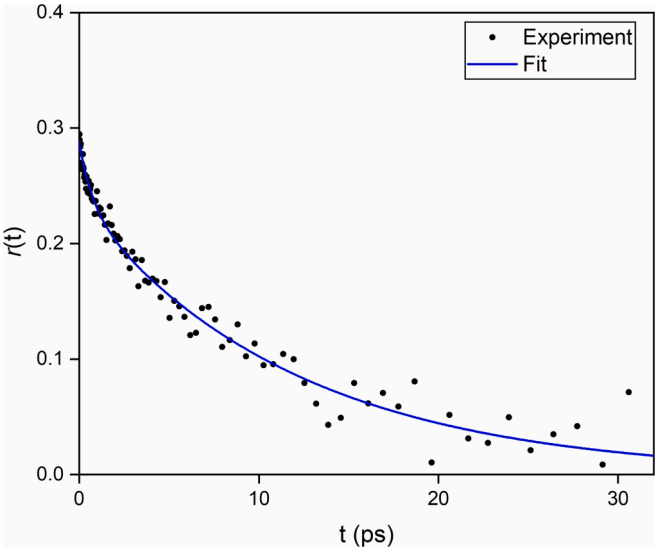

Fig. 6. Orientational relaxation (anisotropy) decay obtained from PSPP experiments (black dots) and the fit using a bi-exponential function (blue) r = 0.05 exp (-t/1) + 0.24 exp (-t/11.9), $R^2 = 0.96$.

The similarity in the slow timescales of the thiocyanate ion's orientational relaxation and spectral diffusion of the solvent is informative. These timescales, measured from two different experiments cannot be directly compared because the experiments measure different correlation functions. However, such a similarity in the two timescales has been previously reported and has been linked to the same underlying physical motions.[49] Therefore, the similarity between the two observables for SCN^- in PC reveals that their time dependencies are controlled by similar processes. A future computational study involving MD simulations study can elucidate the molecular origin of this dependency.

5. Conclusion

Experimental observation of the small ionic probe's solvation structure and dynamics in an organic electrolyte, PC, is reported in the above article. An apparent blue-shift and asymmetry are observed in the FTIR spectrum of the CN stretch in PC with respect to that in DMF and DMSO. The asymmetry has been previously ascribed to NCE which is generally associated with modification of transition dipole moment of the CN stretch probe upon hydrogen bond formation. However, PC is not expected to form any traditional hydrogen bond with the thiocyanate anion. Results from ab initio quantum chemical calculations and MD simulations suggest a small percentage of the solute population can possibly form a weak non-canonical CH…N hydrogen bond in PC. However, further high level theoretical calculations are needed to confirm such a specific interaction.

Solvation dynamics timescales are reported from T_w-dependent 2D IR spectra. NLS analysis of the 2D IR spectra predicts two distinct

timescales of solvation dynamics. The fast and slow timescales have been assigned to the local solvent fluctuations around the solute and the bulk solvent dynamics, respectively. Furthermore, the reorientation dynamics timescale shows signature of wobbling-in-a-cone dynamics. The similarity between the bulk solvent dynamics (spectral diffusion) and the solute's orientational relaxation signifies that similar processes control both dynamics. In the future, this study can be extended to multiple organic electrolytes to obtain a comparative molecular-level understanding of their solvation structure and dynamics.

Data availability

Data are available upon reasonable request.

CRediT authorship contribution statement

Shivshankar Kore: Software, Methodology, Investigation, Formal analysis, Writing – original draft, Writing – review & editing. **Rudhi Ranjan Sahoo:** Writing – original draft, Methodology, Investigation, Formal analysis. **Binit Santra:** Methodology, Investigation, Formal analysis, Writing – original draft. **Archishman Sarkar:** Software, Investigation, Formal analysis, Writing – original draft, Writing – review & editing. **Tubai Chowdhury:** Methodology, Investigation. **Samadhan H. Deshmukh:** Methodology, Investigation. **Sulagna Hazarika:** Investigation. **Srijan Chatterjee:** Conceptualization, Writing – original draft, Writing – review & editing. **Sayan Bagchi:** Supervision, Conceptualization, Writing – review & editing.

Declaration of Competing Interest

The authors declare that they have no known competing financial interests or personal relationships that could have appeared to influence the work reported in this paper.

Data availability

Data will be made available on request.

Acknowledgements

SB acknowledges CSIR-NCL and SERB, India (EMR/2016/000576), for financial support. The authors acknowledge the computational facilities at CSIR-NCL. The authors also acknowledge the National Supercomputing Mission (NSM) for providing computing resources of "PARAM Brahma" at IISER Pune, which is implemented by C-DAC and supported by the Ministry of Electronics and Information Technology (MeitY) and Department of Science and Technology (DST), Government of India. SK acknowledges DBT, RRS acknowledges KVPY fellowship, BS acknowledges DST Inspire, AS acknowledges IACS for the fellowship, SHD and TC acknowledges CSIR for research fellowships.

Appendix A. Supplementary data

Supplementary data to this article can be found online at https://doi.org/10.1016/j.jphotochem.2023.114666.

References

[1] B. Schäffner, et al., Organic Carbonates as Solvents in Synthesis and Catalysis, Chem. Rev. 110 (2010) 4554–4581.
[2] O.O. Postupna, et al., Microscopic Structure and Dynamics of LiBF4 Solutions in Cyclic and Linear Carbonates, J. Phys. Chem. B 115 (49) (2011) 14563.
[3] K.D. Fulfer, D.G. Kuroda, Solvation Structure and Dynamics of the Lithium Ion in Organic Carbonate-Based Electrolytes: A Time-Dependent Infrared Spectroscopy Study, J. Phys. Chem. C 120 (42) (2016) 24011.
[4] J.-D. Xie, et al., Highly concentrated carbonate electrolyte for Li-ion batteries with lithium metal and graphite anodes, J. Power Sources 450 (2020), 227657.
[5] S.I. Smedley, The Interpretation of Ionic Conductivity in, Liquids. 195 (1980).
[6] K. Kondo, et al., Conductivity and Solvation of Li+ Ions of LiPF6 in Propylene Carbonate Solutions, J. Phys. Chem. B 104 (20) (2000) 5040.
[7] M.S. Ding, et al., Change of Conductivity with Salt Content, Solvent Composition, and Temperature for Electrolytes of LiPF6 in Ethylene Carbonate-Ethyl Methyl Carbonate, J. Electrochem. Soc. 148 (10) (2001) A1196.
[8] S.R. Galle Kankanamge, D.G. Kuroda, Molecular structure, chemical exchange, and conductivity mechanism of high concentration litfsi electrolytes, J. Phys. Chem. B 124 (2020) 1965.
[9] J. Lim, et al., Two-Dimensional Infrared Spectroscopy and Molecular Dynamics Simulation Studies of Nonaqueous Lithium Ion Battery Electrolytes, J. Phys. Chem. B 123 (31) (2019) 6651–6663.
[10] J.M. Tarascon, M. Armand, Issues and Challenges Facing Rechargeable Lithium Batteries, Nature 414 (6861) (2001) 359.
[11] K. Xu, Nonaqueous Liquid Electrolytes for Lithium-Based Rechargeable Batteries, Chem. Rev. 104 (10) (2004) 4303.
[12] M.G. Giorgini, et al., Solvation Structure around the Li+ Ion in Mixed Cyclic/Linear Carbonate Solutions Unveiled by the Raman Noncoincidence Effect, J. Phys. Chem. Lett. 6 (16) (2015) 3296.
[13] N. Xin, et al., Solubilities of six lithium salts in five non-aqueous solvents and in a few of their binary mixtures, Fluid Phase Equilib. 461 (2018) 1.
[14] Y.M. Delavoux, et al., Intermolecular structure and hydrogen-bonding in liquid 1,2-propylene carbonate and 1,2-glycerol carbonate determined by neutron scattering, Phys. Chem. Chem. Phys. 19 (2017) 2867–2876.
[15] M.I. Chaudhari, et al., Scaling Atomic Partial Charges of Carbonate Solvents for Lithium Ion Solvation and Diffusion, J. Chem. Theory Comput. 12 (2016) 5709–5718.
[16] A.E. Eisenhart, T.L. Beck, Quantum Simulations of Hydrogen Bonding Effects in Glycerol Carbonate Electrolyte Solutions, J. Phys. Chem. B 125 (2021) 2157–2166.
[17] J.-C. Soetens, et al., Molecular dynamics simulation and X—ray diffraction studies of ethylene carbonate, propylene carbonate and dimethyl carbonate in liquid phase, J. Mol. Liq. 92 (2001) 201–216.
[18] E. Eckstein, et al., X-ray scattering study and molecular simulation of glass forming liquids: Propylene carbonate and salol, J. Chem. Phys. 113 (11) (2000) 4751–4762.
[19] Y. Wang, P.B. Balbuena, Associations of Alkyl Carbonates: Intermolecular C−H···O Interactions, J. Phys. Chem. A 105 (2001) 9972–9982.
[20] K.K. Lee, et al., Ultrafast Fluxional Exchange Dynamics in Electrolyte Solvation Sheath of Lithium Ion Battery, Nat. Commun. 8 (2017) 14658.
[21] Y. Chae, et al., Lithium-Ion Solvation Structure in Organic Carbonate Electrolytes at Low Temperatures, J. Phys. Chem. Lett. 13 (33) (2022) 7881–7888.
[22] B. Dereka, et al., Exchange-Mediated Transport in Battery Electrolytes: Ultrafast or Ultraslow? J. Am. Chem. Soc. 144 (19) (2022) 8591–8604.
[23] M. Ji, S. Park, K.J. Gaffney, Dynamics of Ion Assembly in Solution: 2DIR Spectroscopy Study of LiNCS in Benzonitrile, J. Phys. Chem. Letters 1 (12) (2010) 1771–1775.
[24] D. Ghosh, et al., Association-Dissociation Dynamics of Ionic Electrolytes in Low Dielectric Medium, J. Phys. Chem. B 126 (1) (2022) 239–248.
[25] K.D. Fulfer, D.G. Kuroda, A Comparison of the Solvation Structure and Dynamics of the Lithium Ion in Linear Organic Carbonates with Different Alkyl Chain Lengths, Phys. Chem. Chem. Phys. 19 (36) (2017) 25140.
[26] C. Liang, K. Kwak, M. Cho, Revealing the Solvation Structure and Dynamics of Carbonate Electrolytes in Lithium-Ion Batteries by Two-Dimensional Infrared Spectrum Modeling, J. Phys. Chem. Lett. 8 (23) (2017) 5779.
[27] C. Lim, et al., Solvation Structure around Li+ Ions in Organic Carbonate Electrolytes: Spacer-Free Thin Cell IR Spectroscopy, Anal. Chem. 93 (37) (2021) 12594–12601.
[28] J.D. Forero-Saboya, et al., Cation Solvation and Physicochemical Properties of Ca Battery Electrolytes, J. Phys. Chem. C 123 (49) (2019) 29524–29532.
[29] R. Yuan, C. Yan, M. Fayer, Ion-Molecule Complex Dissociation and Formation Dynamics in LiCl Aqueous Solutions from 2D IR Spectroscopy, J. Phys. Chem. B 122 (46) (2018) 10582–10592.
[30] D. Ghosh, et al., Two Dimensional Infrared Spectroscopy: A Structure Sensitive Technique with Ultrafast Time Resolution, in: D.K. Singh, M. Pradhan, A. Materny (Eds.), Modern Techniques of Spectroscopy: Basics, Instrumentation, and Applications, Springer Singapore, Singapore, 2021, pp. 39–56.
[31] S. Chatterjee, et al., Hydrocarbon Chain-Length Dependence of Solvation Dynamics in Alcohol-Based Deep Eutectic Solvents: A Two-Dimensional Infrared Spectroscopic Investigation, J. Phys. Chem. B 123 (44) (2019) 9355–9363.
[32] J. Tirado-Rives, W.L. Jorgensen, Performance of B3LYP Density Functional Methods for a Large Set of Organic Molecules, J. Chem. Theory Comput. 4 (2) (2008) 297–306.
[33] Frisch, M., et al., *Gaussian Inc.* Wallingford Ct, 2009. **2**.
[34] M.J. Abraham, et al., GROMACS: High Performance Molecular Simulations Through Multi-Level Parallelism From Laptops to Supercomputers, Softwarex 1 (2015) 19.
[35] W.L. Jorgensen, D.S. Maxwell, J. Tirado-Rives, Development and Testing of the OPLS All-Atom Force Field on Conformational Energetics and Properties of Organic Liquids, J. Am. Chem. Soc. 118 (45) (1996) 11225–11236.
[36] M. Brehm, B. Kirchner, TRAVIS - A Free Analyzer and Visualizer for Monte Carlo and Molecular Dynamics Trajectories, J. Chem. Inf. Model. 51 (8) (2011) 2007–2023.
[37] S. Bagchi, S.D. Fried, S.G. Boxer, A Solvatochromic Model Calibrates Nitriles' Vibrational Frequencies to Electrostatic Fields, J. Am. Chem. Soc. 134 (2012) 10373.
[38] A.T. Fafarman, et al., Decomposition of Vibrational Shifts of Nitriles into Electrostatic and Hydrogen-Bonding Effects, J. Am. Chem. Soc. 132 (2010) 12811.

[39] P. Deb, et al., Correlating Nitrile IR Frequencies to Local Electrostatics Quantifies Noncovalent Interactions of Peptides and Proteins, J. Phys. Chem. B 120 (17) (2016) 4034–4046.
[40] J.B. Weaver, et al., Nitrile Infrared Intensities Characterize Electric Fields and Hydrogen Bonding in Protic, Aprotic, and Protein Environments, J. Am. Chem. Soc. 144 (2022) 7562–7567.
[41] P. Deb, et al., Correlating Nitrile IR Frequencies to Local Electrostatics Quantifies Noncovalent Interactions of Peptides and Proteins, J. Phys. Chem. B 120 (2016) 4034.
[42] H. Hao, et al., Structural Dynamics of Short Ligands on the Surface of ZnSe Semiconductor Nanocrystals, J. Phys. Chem. Lett. 13 (14) (2022) 3158–3164.
[43] S.H. Deshmukh, et al., Ligand Dynamics Time Scales Identify the Surface-Ligand Interactions in Thiocyanate-Capped Cadmium Sulfide Nanocrystals, J. Phys. Chem. Lett. 13 (13) (2022) 3059–3065.
[44] Y.S. Kim, R.M. Hochstrasser, Chemical Exchange 2D IR of Hydrogen-Bond Making and Breaking, Proc. Natl. Acad. Sci. U. S. A. 102 (2005) 11185.
[45] B.A. Lindquist, S.A. Corcelli, Nitrile Groups as Vibrational Probes: Calculations of the C≡N Infrared Absorption Line Shape of Acetonitrile in Water and Tetrahydrofuran, J. Phys. Chem. B 112 (20) (2008) 6301–6303.
[46] S.S. Sakpal, et al., Transition of a Deep Eutectic Solution to Aqueous Solution: A Dynamical Perspective of the Dissolved Solute, J. Phys. Chem. Lett. 12 (2021) 8784.
[47] S.D. Fried, S. Bagchi, S.G. Boxer, Measuring electrostatic fields in both hydrogen-bonding and non-hydrogen-bonding environments using carbonyl vibrational probes, J. Am. Chem. Soc. 135 (2013) 11181.
[48] J.R. Schmidt, S.A. Corcelli, J.L. Skinner, Pronounced non-Condon effects in the ultrafast infrared spectroscopy of water, J. Chem. Phys. 123 (4) (2005), 044513.
[49] S.A. Yamada, et al., Dynamics in a Room-Temperature Ionic Liquid from the Cation Perspective: 2D IR Vibrational Echo Spectroscopy, J. Am. Chem. Soc. 139 (6) (2017) 2408–2420.
[50] R. Yuan, et al., Molecular Anion Hydrogen Bonding Dynamics in Aqueous Solution, J. Phys. Chem. B 119 (42) (2015) 13407–13415.
[51] A.L. Webber, et al., Weak Intermolecular CH···N Hydrogen Bonding: Determination of 13CH–15N Hydrogen-Bond Mediated J Couplings by Solid-State NMR Spectroscopy and First-Principles Calculations, J. Phys. Chem. A 124 (3) (2020) 560–572.
[52] K. Shivakumar, et al., Strength from weakness: The role of CH…N hydrogen bond in the formation of wave-like topology in crystals of aza-heterocycles, CrstEngComm 14 (2) (2012) 519–524.
[53] Shirhatti, P.R., et al., *C H···N Hydrogen-Bonding Interaction in 7-Azaindole:CHX3 (X=F, Cl) Complexes.* ChemPhysChem, 2014. **15**(1): p. 109-117.
[54] G.A. Jeffrey, An Introduction to Hydrogen Bonding, Oxford University Press, 1997.
[55] V.A. Koverga, et al., Local structure and hydrogen bonding in liquid γ-butyrolactone and propylene carbonate: A molecular dynamics simulation, J. Mol. Liq. 287 (2019), 110912.
[56] K. Kwak, et al., Frequency-Frequency Correlation Functions and Apodization in Two-Dimensional Infrared Vibrational Echo Spectroscopy: A New Approach, J. Chem. Phys. 127 (12) (2007), 124503.
[57] Z.A. Al-Mualem, C.R. Baiz, Generative Adversarial Neural Networks for Denoising Coherent Multidimensional Spectra, J. Phys. Chem. A 126 (23) (2022) 3816–3825.
[58] M.A. Kahlow, et al., Femtosecond resolved solvation dynamics in polar solvents, J. Chem. Phys. 90 (1) (1989) 151–158.
[59] L.J.G.W. van Wilderen, et al., Vibrational dynamics and solvatochromism of the label SCN in various solvents and hemoglobin by time dependent IR and 2D-IR spectroscopy, Phys. Chem. Chem. Phys. 16 (36) (2014) 19643–19653.
[60] K.K. Lee, et al., Ion-Pairing Dynamics of Li+ and SCN– in Dimethylformamide Solution: Chemical Exchange Two-Dimensional Infrared Spectroscopy, J. Chem. Phys. 134 (2011), 064506.
[61] R. Yuan, M.D. Fayer, Dynamics of Water Molecules and Ions in Concentrated Lithium Chloride Solutions Probed with Ultrafast 2D IR Spectroscopy, J. Phys. Chem. B 123 (2019) 7628.